Journal of Colloid and Interface Science 602 (2021) 207–221

Contents lists available at ScienceDirect

Journal of Colloid and Interface Science

journal homepage: www.elsevier.com/locate/jcis

Regular Article

Air-water interfacial behaviour of whey protein and rapeseed oleosome mixtures

Jack Yang [a,b,c], Leonie C. Waardenburg [b], Claire C. Berton-Carabin [d,e], Constantinos V. Nikiforidis [c], Erik van der Linden [a,b], Leonard M.C. Sagis [b,*]

[a] TiFN, Nieuwe Kanaal 9A, 6709 PA Wageningen, the Netherlands
[b] Laboratory of Physics and Physical Chemistry of Foods, Wageningen University, Bornse Weilanden 9, 6708WG Wageningen, the Netherlands
[c] Laboratory of Biobased Chemistry and Technology, Wageningen University, Bornse Weilanden 9, 6708WG Wageningen, the Netherlands
[d] Laboratory of Food Process Engineering, Wageningen University, Bornse Weilanden 9, 6708WG Wageningen, the Netherlands
[e] INRAE, UR BIA, F-44316 Nantes, France

GRAPHICAL ABSTRACT

Schematic representation (top view from the air phase) of air-water interfaces stabilised by

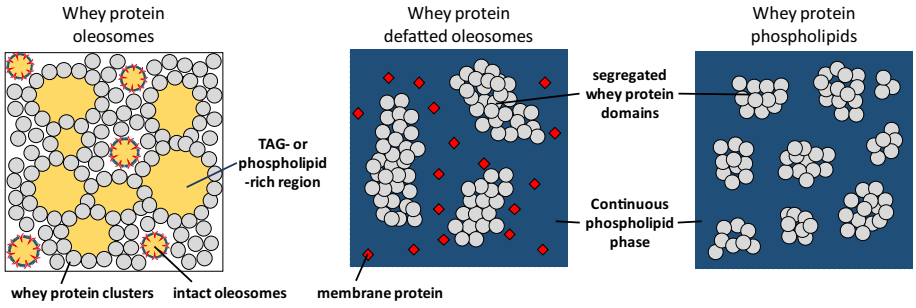

ARTICLE INFO

Article history:
Received 2 February 2021
Revised 13 April 2021
Accepted 28 May 2021
Available online 30 May 2021

Keywords:
Oleosomes
Lipid droplets
Oil bodies
Protein
Phospholipid
Rapeseed
Surface rheology
Atomic force microscopy

ABSTRACT

Hypothesis: Plant seeds store lipids in oleosomes, which are storage organelles with a triacylglycerol (TAG) core surrounded by a phospholipid monolayer and proteins. Due to their membrane components, oleosomes have an affinity for the air/oil–water interface. Therefore, it is expected that oleosomes can stabilise interfaces, and also compete with proteins for the air–water interface. *Experiments:* We mixed rapeseed oleosomes with whey protein isolate (WPI), and evaluated their air–water interfacial properties by interfacial rheology and microstructure imaging. To understand the contribution of the oleosome components to the interfacial properties, oleosome membrane components (phospholipids and membrane proteins) or rapeseed lecithin (phospholipids) were also mixed with WPI. *Findings*: Oleosomes were found to disrupt after adsorption, and formed TAG/phospholipid-rich regions with membrane fragments at the interface, forming a weak and mobile interfacial layer. Mixing oleosomes with WPI resulted in an interface with TAG/phospholipid-rich regions surrounded by whey protein clusters. Membrane components or lecithin mixed with proteins also resulted in an interface where WPI molecules aggregated into small WPI domains, surrounded by a continuous phase of membrane components or phospholipids. We

Abbreviations: OS, oleosome; DOS, defatted oleosome; RPL, rapeseed phospholipid; WPI, whey protein isolate; TAG, triacylglycerol; SDS, sodium dodecyl sulphate; SDS-PAGE, sodium dodecyl sulphate polyacrylamide gel electrophoresis; LAOD, large amplitude oscillatory dilatation; LAOS, large amplitude oscillatory shear; DWR, double wall ring; LB, Langmuir-Blodgett; AFM, atomic force microscopy; LVE, linear viscoelastic regime; NLVE, nonlinear viscoelastic regime; LE, liquid expanded; LC, liquid condensed.

* Corresponding author.
E-mail address: leonard.sagis@wur.nl (L.M.C. Sagis).

https://doi.org/10.1016/j.jcis.2021.05.172

also observed an increase in stiffness of the interfacial layer, due to the presence of oleosome membrane proteins at the interface.

1. Introduction

Plant oilseeds, such as soybeans, rapeseeds, and sunflower seeds, are cultivated worldwide for their oils. In plant oilseeds, lipids are present in storage organelles, called oleosomes (OS, also known as oil bodies or lipid droplets) [1]. OS are natural oil droplets with a triacylglycerol (TAG) core that is surrounded by a monomeric membrane layer, consisting of a phospholipid monolayer with anchored proteins [2–4] (Fig. 1). The diameter of OS ranges from 0.2 to 10 μm, depending on the plant source and environmental conditions during cultivation [2,5]. Currently, OS are disrupted with mechanical treatments and organic solvents to extract the TAG core for the production of plant oils for food purposes. A side product from oil production are phospholipids, which are commercially known as lecithin. Phospholipids are widely applied as emulsifiers to stabilise oil droplets or other colloidal structures in the food, cosmetical, and pharmaceutical industry [6]. A new upcoming trend is the so-called minimal processing of ingredients to decrease the environmental impact of the purification process [7–9]. Pure phospholipids are obtained through extensive refinery and thus is not environmentally friendly. In contrast, the direct use of natural oil droplets, OS, would be much more environmentally friendly compared to pure phospholipids.

OS has several other promising features, such as a high physical and chemical stability against lipid oxidation and droplet coalescence [10–13] due to the protective protein-phospholipid membrane, where surface proteins and phospholipids interact through hydrophobic and electrostatic forces. The most abundant phospholipids in plant OS membranes are phosphatidylcholine and phosphatidylserine [5]. Next to phospholipids, three types of membrane proteins are found in the interface of OS, which are oleosins, caleosins, and steroleosins, with oleosin being by far the most abundant one [1,3]. The outer surface of the OS is hydrophilic, due to the polar phospholipid headgroups and membrane protein hydrophilic domains being directed outwards [4]. The overall hydrophilicity of the OS' surface allows an aqueous extraction from plant material, which is often performed by soaking, and disruption of cell walls, followed by separation of solids from the aqueous phase [14–16].

Many functionality studies have been performed on OS as a natural oil droplet with high chemical and physical stability [10,11,17,18]. Another potential application could be the role of emulsifier/surfactant, which was demonstrated by several studies for OS from different sources. Ishii et al. showed the possibility to stabilise emulsions by mixing soybean OS and free oil, and showed the OS monolayer can expand, allowing the OS to take up free oil [14]. The same was also demonstrated for sunflower seed OS, which were disrupted upon homogenisation, and fragments of membrane material formed an interfacial layer around the oil droplets [18]. The unfolding of soybean OS at the air–water interface was investigated by Waschatko et al.[19,20], and revealed rupture of the OS after adsorption, which is presumably followed by structural rearrangement of the interfacial components (phospholipids, membrane proteins, and TAGs) over time. Furthermore, Deleu et al. revealed that both phospholipids and OS proteins play an important role in emulsion stabilisation, as phospholipids were able to form small oil droplets and prevent flocculation due to a high negative surface charge. Additionally, the presence of membrane proteins provided oil droplet stability against coalescence [21].

The interface stabilising properties of the OS and their membrane components are not well understood yet. Therefore, we aimed to perform an extensive characterisation of the interface stabilising properties of OS from rapeseed, which are one of the most cultivated oilseeds worldwide and contain about 40% (w/w) oil [22]. To further investigate their interfacial stabilisation mechanisms, the OS were defatted to obtain OS membranes. Additionally, we included a commercially available rapeseed phospholipid extract (lecithin), which was derived from the OS membranes of defatted seeds. As foods are complex multi-component systems, other surface-active components will co-exist with OS, possibly influencing the interfacial layer formation. An example is proteins, a commonly used emulsifier, which could influence the interface stabilising behaviour of OS, and vice versa [23]. As exogeneous

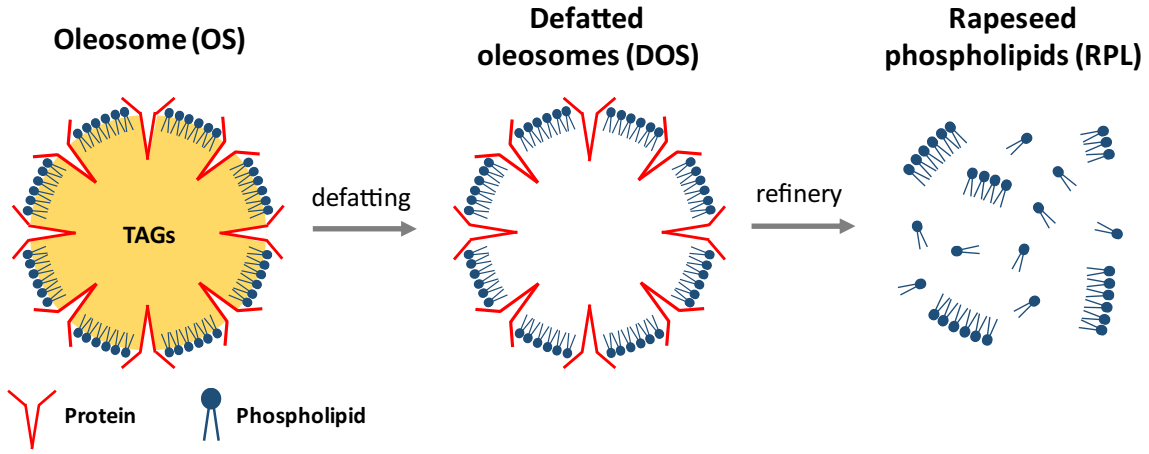

Fig. 1. A schematic structure of the studied materials in this work: oleosomes, dried and defatted oleosomes, and rapeseed phospholipids in dried state. The components of the illustrations are not to scale.

proteins and OS mixtures have not yet been studied, we specifically addressed this matter. The OS were mixed with a model whey protein isolate (WPI) system, as the structural and functional (interfacial) properties of these proteins are well characterized [24,25].

In summary, we first studied the air–water interface stabilising properties of the rapeseed phospholipids (RPL), followed by those of a less refined system, the defatted oleosomes (DOS), and finally of the OS. The components were mixed with WPI to assess the interfacial properties of the mixtures. The interfacial properties were evaluated using large amplitude oscillatory dilatational (LAOD) and shear (LAOS) rheology. The topography of the interfacial films was characterised by atomic force microscopy (AFM) on Langmuir-Blodgett films. Our work provides valuable insights into the interface stabilising mechanism of OS, and of OS in combination with exogenous proteins. The findings in this work allow the further exploitation of oleosomes as a food ingredient and interface stabiliser in multiphase food systems, such as foams and emulsions.

1.1. Experimental section

1.1.1. Materials

Alizze rapeseeds were obtained from a European seed producer. Rapeseed phospholipids (commercial lecithin) (Emulpur RS Lecithin, Cargill, France), whey protein isolate (WPI) (BiPro, Davisco Food international, France), and other chemicals (Sigma-Aldrich, USA) were all used as received. Ultrapure water (MilliQ Purelab Ultra, Germany) was used for all experiments.

1.2. Sample preparation

1.2.1. Oleosomes extraction

The oleosome extraction method was based on previous work by Romero-Guzmán et al., with several adaptations [26]. Rapeseeds were dispersed in ultrapure water at a 1:10 (w/v) ratio. The pH was adjusted to 9.0 with 1 M NaOH and the dispersion was stirred for 4 h, while constantly adjusting the pH to 9.0. After soaking, the dispersion was blended for 1 min at maximum speed in a kitchen blender (Waring Commercial, 400 W, USA). The slurry was passed through a cheesecloth to remove the solids. The pH of the filtrate was adjusted to 9.0 and the filtrate was centrifuged at 10,000xg at 4 °C for 30 min. The cream layer was collected and resuspended in ultrapure water at a 1:5 (w/v) ratio. The dispersion was stirred for 15 min and centrifuged at 10,000xg at 4 °C for 30 min. The washing step and centrifugation step were once more repeated with buffer (sodium phosphate, 20 mM, pH 7.0) instead of ultrapure water. The oleosome extract was diluted with buffer based on dry matter content and used in experiments for a maximum of 5 days with the addition of sodium azide and storage at 4 °C.

1.2.2. Defatting of oleosomes

Oleosomes were diluted in ultrapure water in an 1:10 (w/v) ratio, frozen using liquid nitrogen, and freeze-dried. The freeze-dried oleosomes were defatted by adding hexane in a 1:10 (w/v) ratio, followed by 2 h stirring at room temperature, and filtering over filtration paper. The defatting steps were repeated three more times. The final residue was dried overnight in a desiccator while constantly being flushed with nitrogen gas.

1.2.3. Compositional analysis

1.2.3.1. Protein content. The protein content was determined by measuring the nitrogen content using a Flash EA 1112 Series Dumas (Interscience, The Netherlands). The nitrogen content was converted into a protein content with a conversion factor of 5.7 [27].

1.2.3.2. Lipid content. The lipid content of the oleosomes was determined by solvent (petroleum ether) extraction using a Soxhlet. The oleosomes were dried overnight at 60 °C, followed by solvent extraction for 6 h. The lipid content was determined by weighing the initial sample and the lipids in the collection flasks. The measurements were performed in duplicate.

1.2.4. Dissolving samples

Whey protein isolate (WPI) was dissolved at 2.5% (w/w) in buffer (sodium phosphate, 20 mM, pH 7.0) for 4 h and centrifuged at 16,000xg for 30 min. The supernatant was passed through a 0.45 μm syringe filter and the filtrate was diluted based on the dry matter content. Rapeseed phospholipids (commercial lecithin) and defatted oleosomes were dispersed in the buffer by stirring the sample for 2 h at room temperature, followed by high speed mixing in an Ultra-Turrax (IKA, USA) at 8,000 rpm for 10 s, and hydrated overnight at 4 °C.

1.2.5. Preparation of mixtures

For the majority of the experiments, a WPI solution with a fixed concentration of 0.2% (w/w) was mixed with a 0.2% (w/w) oleosome, defatted oleosome, or rapeseed phospholipid suspension in a 1:1 (v/v) ratio, which resulted in a final concentration of 0.1% (w/w) of all components. The mixture was carefully stirred with a magnetic rod on a stirrer plate for 5 min. When concentrations deviated from this, it will be mentioned in the following sections.

1.3. Determination of droplet size distribution

The droplet size distribution of the oleosomes dispersions was characterised by static laser light scattering using a Mastersizer 2000 equipment (Malvern Instruments, UK). The refractive indices were 1.469 for the dispersed phase (oleosomes) and 1.330 for the dispersant (water). Potential flocculation was assessed by diluting the sample in a 1:1 (v/v) ratio with a 1% (w/w) sodium dodecyl sulphate (SDS) solution. Two independent oleosome batches were produced, and each sample was measured three times.

1.4. Determination of adsorption behaviour and surface dilatational properties

1.4.1. Adsorption behaviour, frequency sweeps, and step dilatation

The interfacial properties of the air–water interface, stabilised by the various components, and their mixtures, were studied with drop tensiometry. Time sweeps, frequency sweeps, and step-dilatations were performed in a PAT-1 M drop tensiometer (Sinterface Technologies, Germany). The protein solution was injected through a hollow needle to create a hanging droplet (area of 20 mm^2) at the tip of a needle. The contour of the droplet was fitted with the Young-Laplace equation to obtain the surface tension. Before deformations, the droplet was equilibrated for 3 h while monitoring the surface tension. Frequency sweeps were performed by varying the oscillatory frequency from 0.002 to 0.1 Hz with an amplitude of 3%. Each frequency cycle was performed with 5 sinusoidal oscillations followed by a rest step with the duration of a full oscillation. Step dilatation experiments were performed by extending or compressing the area of the interface by 10% with a step time of 2 s. All measurements were performed at least in triplicate at 20 °C.

1.4.2. Amplitude sweeps

Amplitude sweeps of the interfacial layer were performed using an ADT (Teclis, France), which was operated similarly to the PAT.

The main difference was the size of the hanging droplet (area of 15 mm^2) and the type of needle (G18). After 3 h of waiting time, the droplet was subjected to various amplitudes (3–50%) at a frequency of 0.02 Hz. Each amplitude cycle was performed with 5 sinusoidal oscillations followed by a rest step of 50 s. All measurements were performed at least in triplicate at 20 °C.

1.4.3. Analysis of large amplitude oscillatory dilatational experiments

The amplitude sweep data were visualised by plotting Lissajous curves of the surface pressure ($\Pi(t) = \gamma(t)-\gamma_0$) versus deformation ($(A(t)-A_0)/A_0$). Here, $\gamma(t)$ and $A(t)$ are the surface tension and area of the deformed interface at time t, and γ_0 and A_0 are the surface tension and area of the non-deformed interface. Lissajous plots were made from the middle three oscillations of each amplitude cycle.

1.5. Determination of surface shear properties

The surface shear properties of the interfaces were determined using a double-wall-ring (DWR) geometry coupled to an AR-G2 rheometer (TA Instruments, USA). The diamond-edged ring of the DWR was positioned at the air–water interface of the sample in a double-wall Teflon trough and covered with a vapour cap to limit evaporation. The interface was pre-sheared for 5 min at a shear rate of 10/s, and equilibrated for 3 h before a strain or frequency sweep. The strain sweeps were performed with strains varying from 0.01 to 100% at a frequency of 0.1 Hz, and the frequency sweeps were performed with frequencies varying from 0.01 to 10 Hz at a strain of 1%. All experiments were performed in triplicate at 20 °C. In all our studied systems, the contribution of the subphase to the stress signal is negligible, as the Boussinesq number (ratio between surface and bulk stress) was greater than 1[28].

1.6. Preparation of Langmuir-Blodgett films

Protein/lipid-stabilised interfaces were deposited on solid substrates to produce Langmuir-Blodgett (LB) films in a Langmuir trough (KSV NIMA/Biolin Scientific Oy, Finland). Samples of pure WPI, oleosome, rapeseed phospholipid, and defatted oleosome contained 0.1% (w/w) material. The WPI-lipid mixtures contained 0.05% (w/w) protein (WPI), and 0.05% (w/w) lipids based on dry matter.

The mixtures of protein with lipid had a protein content of 0.05% (w/w), and a lipid content of 0.05% (w/w). The Langmuir trough was filled with buffer (sodium phosphate, 20 mN, pH 7.0) and 200 μL of the sample were injected in the subphase using a syringe. The samples were allowed to adsorb and equilibrate at the interface for 3 h, while the surface pressure was monitored using a Wilhelmy plate (platinum, perimeter 20 mm, height 10 mm). After equilibration, the interfacial layer was compressed with barriers moving at a speed of 5 mm/min to target surface pressures. The interfacial layer was deposited on a freshly cleaved mica sheet (Highest Grade V1 Mica, Ted Pella, USA) at a withdrawal speed of 1 mm/min. The LB films were dried in a desiccator at room temperature, and all films were produced in duplicate.

1.7. Determination of interfacial microstructure by AFM

The topography of the interfacial microstructure was analysed using atomic force microscopy (AFM, MultiMode 8-HR, Bruker, USA). The LB films were analysed in tapping mode using a Scanasyst-air model non-conductive pyramidal silicon nitride probe (Bruker, USA) with a normal spring constant of 0.40 N/m and a lateral scan frequency of 0.977 Hz was applied on all images. The scan area was 2×2 μm^2 and 10×10 μm^2 with a lateral resolution of 512×512 $pixels^2$. The films were scanned for at least two locations to ensure good representativeness and the images were analysed using Nanoscope Analysis v1.5 software (Bruker, USA).

2. Results and discussion

2.1. Physico-chemical properties of oleosomes

The aqueous extraction method yielded rapeseed oleosomes (OS) with 88.5 ± 3.8% (w/w) lipids, 7.2 ± 0.3% protein, and the remaining 4.3% should mainly consist of phospholipids and minerals. We should also keep in mind that the phospholipids might also be partially extracted with the lipid content determination method. The OS suspension had a broad size distribution at pH 7.0, ranging from 2 to 300 μm with a $d_{3,2}$ of 7.97 ± 0.20 μm (Fig. 2). Sodium dodecyl sulphate (SDS) was added to break up aggregated droplets and revealed smaller droplets ranging from 0.2 to 20 μm with a $d_{3,2}$ of 0.81 ± 0.02 μm. Comparable OS composition and droplet sizes were also demonstrated by Romero-Guzmán et al. for rapeseed oleosomes extracted at a pH value of 7.0 [26] using fluorescence microscopy and light scattering techniques, where the formation of large flocculates was attributed to the low surface charges and the presence of storage proteins [15]. To investigate the efficiency of the OS purification step and the possible presence of rapeseed storage proteins, defatted oleosomes (DOS) were analysed using SDS-PAGE (Fig. 3). The thickest band in the scan is around 16 kDa, which corresponds to the oleosome membrane protein oleosin [5]. The rapeseed storage protein napin and cruciferin were previously found to form bands between 6 and 10 and 18–28 kDa, respectively [29]. As only light bands are shown in these molecular weight regions, we do not expect the storage proteins to play a major role in the interfacial composition and properties.

2.2. Whey protein – rapeseed phospholipid mixtures

2.2.1. Adsorption behaviour of whey protein – rapeseed phospholipid mixtures

First, we studied the interfacial properties of rapeseed phospholipids (RPL) from a commercial lecithin, which were extracted from the oleosome membrane as a side product of plant oil extraction. During oil extraction, the triacylglycerol (TAG) core was extracted using organic solvents, and the remaining membrane is often refined by the removal of the proteins to obtain a pure phospholipid extract (lecithin). The removal of protein is also reflected in

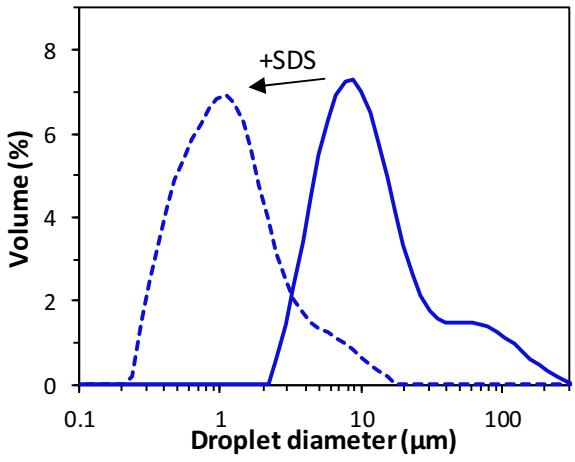

Fig. 2. The volume-based size distribution of oleosomes (solid line) in buffer (20 mM PO_4, pH 7.0). SDS was added to break-up possible aggregates to obtain the single droplet size of the oleosomes (dashed line).

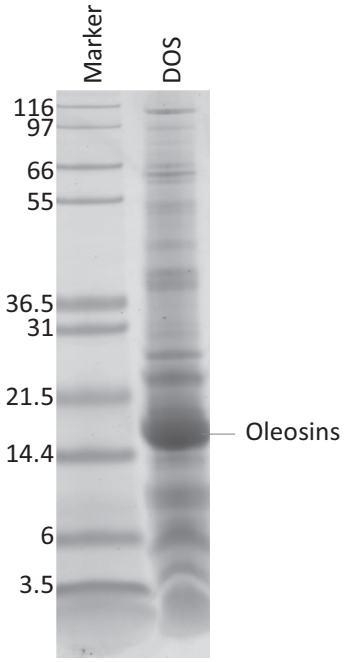

Fig. 3. SDS-PAGE under reducing conditions containing marker with the corresponding molecular weight in kDa on the left, and the defatted oleosomes (DOS) on the right.

the low protein content of 6.9 ± 1.1% (w/w). We should keep in mind that the main phospholipid in the OS membrane, phosphatidylcholine, possesses a choline group, which can contribute to the nitrogen-based protein content. Nonetheless, the protein content gives us a rough estimation of the difference in protein content between the RPL, DOS, and OS.

The surface activity of RPL, whey protein isolate (WPI) and a WPI-RPL mixture at 1:1 (w/w) ratio is shown in Fig. 4. RPL had a lag time of 2 s before the material started to increase the surface pressure. An explanation could be the low solubility of RPL, as evidenced by the fact that the suspension was turbid and material sedimented over time. Additionally, phospholipids are known to form vesicles in water, which might diffuse slowly towards the interface [6]. The surface pressure of RPL increased to a final surface pressure of 25 mN/m after 3 h of adsorption. Whey protein isolate (WPI) showed an immediate surface pressure increase to 8 mN/m, followed by a constant increase to a final value of 20 mN/m. The adsorption of WPI was faster than RPL in the first 70 s, probably due to the low solubility of RPL and slow diffusion of the vesicles. On the other hand, RPL reached higher surface pressures after 70 s, as smaller phospholipids can form a more densely packed interface [30,31]. The interfacial packing efficiency of lipid-like structures is also determined by the chemical structure of the aliphatic tails, as unsaturation in *cis* configuration decrease the packing density [32]. The WPI-RPL mixture led to a similar surface pressure as pure WPI in the first two s, which is similar to the lag phase of pure RPL. Afterwards, the surface pressure increased to slightly higher values compared to pure WPI, but ended again at the same value as WPI after 10,800 s. This could suggest initial adsorption of WPI at the interface, followed by RPL. As less free interfacial area is available for RPL to adsorb on, the surface pressure did not reach the value of 25 mN/m of pure RPL. To further assess the interface stabilising mechanisms of the WPI-OS mixtures, we performed shear and dilatational rheology on the interface.

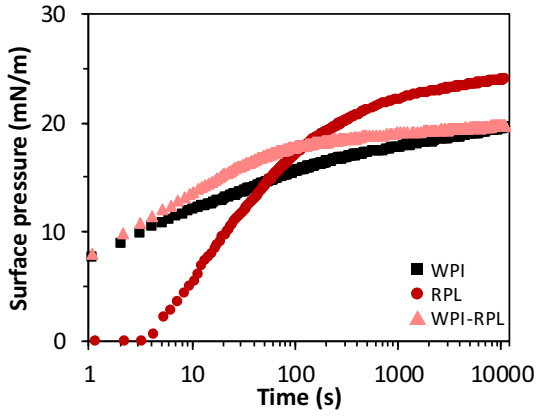

Fig. 4. Surface pressure as a function of time of interfacial films stabilised by WPI (black square), RPL (dark red circle), and WPI-RPL mixtures (light red triangle) in buffer (20 mM PO_4, pH 7.0). The surface pressure isotherms represent an average from at least three replicates. The standard deviation was below 5%. (For interpretation of the references to colour in this figure legend, the reader is referred to the web version of this article.)

2.2.2. Interfacial rheology on whey protein – rapeseed phospholipid stabilised interfaces

The surface shear moduli of interfacial films stabilised by WPI, RPL and WPI-RPL mixtures were measured in a strain sweep using a double wall ring geometry coupled to a rheometer Fig. 5A. The WPI-stabilised interface showed a linear viscoelastic (LVE) regime up to 1% strain, where the storage (G_i') and loss modulus (G_i") remained constant. The G_i' was found to be higher than the G_i" in the LVE, resulting in a tanδ of around 0.24, thus suggesting solid-like behaviour. At larger deformations, the response entered the non-linear viscoelastic (NLVE) regime, as the moduli started to decline, revealing that the applied deformation affected the interfacial microstructure, thus resulting in softening behaviour. The *Gi*" had a weak strain overshoot between 3 and 10% strain, which is presumably related to the simultaneous breakdown and formation of new network junctions, due to the collision of clusters. This behaviour is specified as type III nonlinear behaviour, and is commonly found for soft solids [33]. To summarise, the WPI-stabilised air–water interface clearly showed the rheological behaviour of a viscoelastic solid, as was also more elaborately demonstrated in our previous work [24]. Surface shear experiments were also performed on RPL- and WPI-RPL-stabilised interfaces but resulted in torque values that were lower than the minimum torque limits of the rheometer. This suggests the formation of a very weak interface with limited in-plane interactions between the molecules at the surface.

A comparable effect is present in the amplitude sweep in dilatational deformations (Fig. 5B). The WPI-stabilised interface had a surface dilatational elastic modulus (E_d') that decreased from 84 to 20 mN/m with increasing amplitude, and this amplitude dependency implies the breakdown of the interfacial microstructure upon applied deformation. Different behaviour can be observed for the RPL-stabilised interfaces, which had a constant E_d' up to 20% amplitude, implying a prolonged linear viscoelastic (LVE) regime. At higher deformations, the interfacial microstructure was disrupted, which was reflected in a decrease in elastic modulus. The WPI-RPL mixtures resulted in moduli between 18 and 25 mN/m over the whole range of deformations, which is lower than pure WPI or RPL. The interactions at the interface were further studied by performing frequency sweeps to evaluate the frequency dependence and was quantified using a power-law scaling with frequency, $E_d' \sim \omega^n$. A value of n = 0.5 would suggest that the elasticity of the interface is predominantly affected by the exchange of stabiliser between the bulk and interface [34]. The *n*-values of

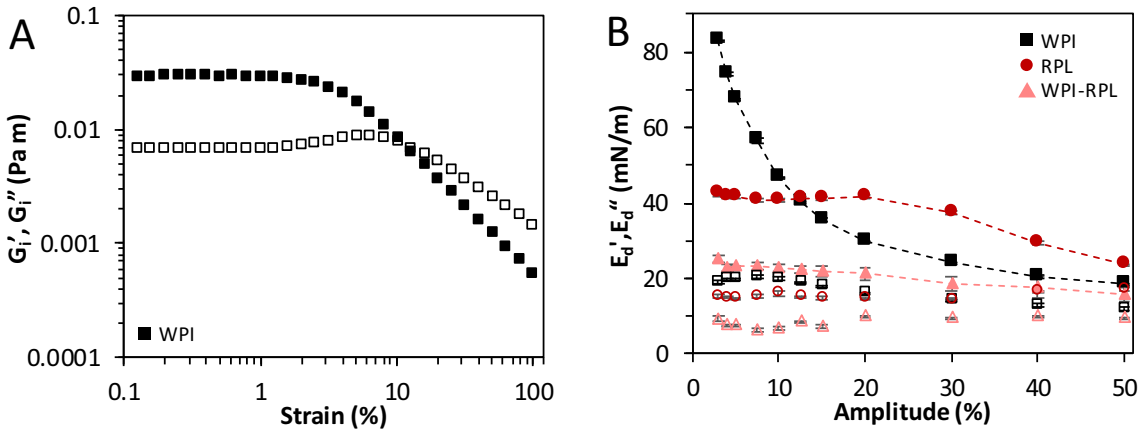

Fig. 5. (A) The surface shear storage (G_i') and loss (G_i") moduli as a function of strain of interfacial films stabilised by WPI (black square). (B) The surface dilatational storage (E_d') and loss (E_d") moduli as a function of amplitude of interfacial films stabilised by WPI (black square), RPL (dark red circle), and WPI-RPL mixtures (light red triangle) in buffer (20 mM PO_4, pH 7.0). Closed symbols show the storage modulus (G_i' or E_d') and open symbols show the loss modulus (G_i" or E_d"). The averages and standard deviations are the result of at least three replicates. (For interpretation of the references to colour in this figure legend, the reader is referred to the web version of this article.)

WPI, RPL and WPI-RPL mixtures were found to be 0.12 ± 0.03, 0.24 ± 0.01, and 0.23 ± 0.03, respectively (Table 1). RPL had an increased frequency dependency, which revealed a more mobile interface compared to WPI. This would also suggest increased transfer between bulk and interface for RPL-stabilised interfaces, where the interfacial stabiliser is pushed into the bulk upon compression of the interface, and stabiliser adsorbs upon creation of new surface area in extension. The higher *n*-value for WPI-RPL compared to WPI also indicate that RPL dominated the rheological properties of the mixtures. The composition of the interface was further examined using Lissajous plots and microstructure imaging.

2.2.3. Lissajous plots and interfacial microstructure imaging

To further assess the mechanical and structural properties of the interfacial films, we generated Lissajous plots using the interfacial stress and deformation from the dilatational deformations, and also studied the interfacial microstructure by performing atomic force microscopy (AFM) on Langmuir-Blodgett (LB) films (Fig. 6). Lissajous plots are proven to be a useful tool in rheology, as they allow for a detailed study of the non-linearities in the stress response [35,36]. The shear and dilatation moduli in Fig. 5 are obtained from the first harmonic of the Fourier transformation of the stress signal, which is a suitable method for measurements in the LVE regime. When the response enters the NLVE regime, higher harmonics are present in the stress response (only odd ones in shear, and even and odd ones in dilatation). Higher harmonics are completely neglected in the first harmonic moduli, but their contribution can be analysed in Lissajous plots by plotting the interfacial stress directly versus the deformation. In earlier work, we demonstrated that microstructure imaging of LB films contributes to a better understanding of the behaviour of interfacial layers [8,24,37].

Table 1
An overview of the value of the power-law exponent n, obtained from the dilatational frequency sweeps, for pure WPI, OS, DOS, and mixture-stabilised interfaces. The averages and standard deviations are the result of at least three replicates.

	n-value
WPI	0.12 ± 0.03
OS	0.30 ± 0.01
WPI-OS	0.18 ± 0.03
DOS	0.30 ± 0.03
WPI-DOS	0.27 ± 0.02
RPL	0.24 ± 0.01
WPI-RPL	0.23 ± 0.05

The samples were infused in the subphase of a Langmuir trough filled with buffer. After 3 h of waiting time (similar to the waiting time in rheology), the diffusion-based film was compressed and transferred to a substrate, creating an LB Blodgett film. In our previous work, a phase transition was found to occur around 21 mN/m in the (Langmuir) surface pressure isotherms of WPI [24]. Surface pressure isotherms have been widely studied for Langmuir films stabilised by small molecular weight surfactants [38]. For interfaces stabilised by the latter, the compression state of the interface before the phase transition is called the liquid expanded (LE) state, where molecules start increasingly interacting and reorienting to a more densely packed layer upon increasing the degree of compression. The region after the phase transition is referred to as a liquid condensed (LC) state [38], where the interfacial stabilisers are compressed into a densely packed interfacial layer. Surface pressure isotherms of the lipids can be observed in Figure S1 in the SI. We produced LB films in the LE and LC state of a WPI-stabilised interfacial layer at surface pressures of 15 and 25 mN/m, respectively [38].

The Lissajous plot obtained from the WPI-stabilised interfacial film had a symmetric and narrow shape at 5% deformation (Fig. 6A), which reveals a linear viscoelastic behaviour, where the elastic component dominates the stress response. At higher deformations, such as 50%, the interfacial structure was disrupted, which caused the Lissajous plots to become asymmetric. The asymmetry helps us to further understand the interfacial network structure. If we start at the maximum compression, so at a deformation of −0.50, we can observe a rapid increase in surface pressure, which indicates a predominantly elastic response. Around a deformation of −0.40, the rapid increase becomes more gradual. This point depicts intra-cycle yielding, where the viscous contribution starts dominating, and the interfacial layer starts flowing. The gradual decrease of the slope of the plot afterwards is called intra-cycle strain softening (in extension). The opposite can be observed in compression, as the surface pressure changed steeply to a higher maximum surface pressure (-20 mN/m) compared to the one in extension (7 mN/m). This behaviour is called intra-cycle strain hardening, which can be attributed to concentrating the proteins (as individual molecules, or supramolecular structures) on the

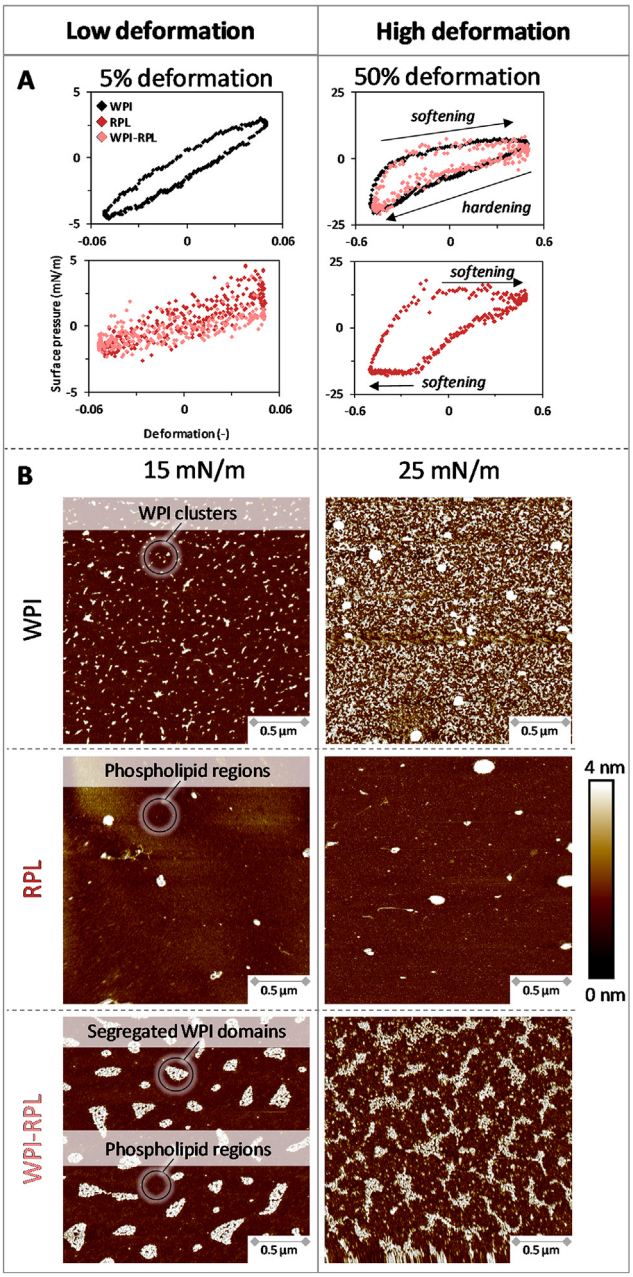

Fig. 6. (A) Lissajous plots of surface pressure as a function of the applied deformation, obtained from amplitude sweeps of air–water interfacial films stabilised by WPI, RPL, and WPI-RPL mixtures. For clarity, one representative plot is shown for each sample, but comparable plots were obtained on at least three replicates. (B) AFM images of Langmuir-Blodgett films made from RPL and WPI-RPL mixtures. The surface pressure indicates the conditions during film sampling.

interface upon compression. As a result, more densely clustered regions will be formed that start jamming at such large deformations.

The jamming of these clusters was nicely depicted in the AFM images in Fig. 6B, as can be observed as white structures on the WPI film at 15 mN/m (which corresponds to an expanded state). The whey protein clusters were formed due to the segregation of proteins at the interface, driven by attractive interactions. Segregation of proteins occurs continuously on the interface and is reflected in the constant increase of surface pressure after the initial adsorption phase of the proteins. Such long-term processes were found to continue even after more than 12 h of ageing of the interface [24,39]. The long time-tail in the adsorption kinetics is often attributed to protein denaturation/unfolding and intra-protein rearrangements [23,40], which seems to be unlikely, as these long-term processes were also obtained for heat-denatured whey proteins [24]. Therefore, other processes such as protein orientational rearrangements and the earlier described segregation of proteins at the interface are more likely to cause the long-term processes that result in the time-tail [37]. At a higher compression to a surface pressure of 25 mN/m (which corresponds to a higher degree of compression), the WPI interfacial film was densely compressed into a more condensed state, where more clusters can be seen on the AFM film. Here, the clusters seemed to start interacting and jamming, which coincides with the strain hardening in compression in the Lissajous plots at 50% deformation amplitude. From these observations, we conclude that the WPI-stabilised interfaces behave as heterogeneous viscoelastic solids.

The Lissajous plots of the RPL-stabilised interface showed notable differences compared to WPI (Fig. 6A). The plot at 5% deformation had a symmetric and very narrow loop, which suggests an almost fully elastic response. The plot for RPL started to display major asymmetries at higher deformations. The plot at 50% deformation had a steep elastic response in extension from −0.50 to −0.20 deformation, followed by intra-cycle yielding around −0.20 deformation. After yielding, a nearly constant surface pressure was observed, which indicates intra-cycle strain softening in extension. A minor degree of strain hardening in compression can be observed, followed by strain softening between −0.20 to −0.50 deformation. Phospholipids are known to possess a complex phase diagram, where phase transitions can occur depending on, for instance, the degree of compression of the interfacial layer [38].

The strain softening in compression could be attributed to three different interfacial phenomena: 1. interfacial domains that start to slide over each other; 2. buckling of the interface; or 3. exchange of molecules between bulk and interface. Buckling seems improbable to occur, as this phenomenon requires strong intramolecular interactions between stabiliser molecules at the interface, which, for instance, were earlier observed for saponin-stabilised interfaces [41,42]. Such strong interactions were not observed for RPL in both shear and dilatational rheology. In the surface pressure isotherms from the Langmuir trough (Figure S1 in SI), RPL showed a phase transition at 36 mN/m, where the slope of the surface pressure isotherm decreases. This point reflected the transition from a liquid expanded (LE) to a liquid condensed (LC) phase, where the phospholipid layer was densely compressed [38], and is also known as a state where the LE and LC phase co-exist. At such high compressions, some expanded regions started to form more condensed and solid-like structures and resulted in the lower slope in the surface pressure isotherm. This phase transition could explain the strain softening behaviour in the Lissajous plots at 50% deformation, and the formed condensed/solid-like interfacial domains could also start to slide over each other at such high compressions. Another explanation could be the exchange of RPL between the interface and the bulk upon compression and extension of the interfacial area, as the RPL displayed weak in-plane interactions at the interface. AFM images of LB films of RPL showed a flat surface with larger structures (Fig. 6B) and could correspond to insoluble material or proteinaceous material. The AFM image remained similar at higher compression (to a surface pressure of 25 mN/m), which could imply that material in the flat areas are either pushed into the bulk upon higher compressions (or pushed below the surface, as AFM only analyses the topography), or started to form a more densely compressed layer that might not be visible within the resolution of the AFM.

Mixing WPI and RPL resulted in a Lissajous plot at 5% deformation, which is more tilted towards the horizontal axis compared to pure WPI (Fig. 6). This is also reflected in a lower E_d' of the WPI-RPL mixture than pure WPI or RPL-stabilised interfaces. In the AFM

image of the LB film at 15 mN/m, more and higher structures are present compared to pure RPL. The structures are assumed to be segregated domains of WPI, which could be surrounded by phospholipids. The latter formed the continuous phase and dominated the interfacial properties, and this would explain the weak interfaces observed in dilatational and shear rheology. Whey proteins also seem to prevent the phospholipids from forming an interface similar to pure RPL, as the moduli of the mixture were substantially lower compared to either pure WPI or RPL. The partial displacement of proteins from a surface by low molecular weight surfactants was previously demonstrated for milk proteins and Tween 20, a non-ionic surfactant [43,44]. In these studies, AFM images on the interfacial microstructure also demonstrated large surfactant-rich regions that surround domains of milk proteins, and resulted in a decrease of surface moduli compared to pure proteins. At higher compressions, the AFM image corresponding to the film at 25 mN/m displayed disordered domains of whey proteins that seemed to start interacting mutually. The interactions involving whey proteins at WPI at a WPI-RPL-stabilised interface can be observed in the Lissajous plot at 50% deformation, which overlaps with the Lissajous plot of pure WPI. At such high deformations, the RPL is likely to be pushed out of the interface, which would allow the whey proteins in WPI-RPL films to start jamming, thus showing a rheological response similar to that of the film with pure WPI. A schematic overview of a whey protein-phospholipid interface is shown in Fig. 7. In summary, the combination of rheology and microstructure imaging on a WPI-RPL mixed interface suggests the formation of whey protein domains, surrounded by a continuous RPL-rich phase. Here, we confirmed the ability of phospholipids to impair the in-plane interactions of proteins.

2.3. Whey protein – defatted oleosome mixtures

2.3.1. Adsorption behaviour and interfacial rheology of whey protein – defatted oleosome mixtures

The complexity of the system was increased by studying defatted oleosomes (DOS), where the TAGs were removed from the OS. The RPL is a refined extract from the DOS, and the major compositional difference is the presence of membrane proteins in the DOS, as reflected in protein content of 69.5 ± 0.3% (w/w). We also expect a structural difference between RPL and DOS, as was previously demonstrated for sunflower DOS, which was found to exist as empty membrane shells of OS using scanning electron microscopy [18]. RPL is more likely to be disrupted in the phospholipid refinery process. However, we should be cautious with the assumptions on the DOS structure, as the sunflower DOS were analysed in a dry state, and these empty OS membrane shells could be disrupted upon dissolution in a polar environment. The presence of free phospholipids and membrane protein would be thermodynamically unfavourable due to their amphiphilicity. Therefore, it would be likely that these components form micelles, vesicles or protein aggregates upon disruption. The remaining 30.5% was expected to mainly consist of phospholipids. DOS were previously found to be surface-active, as emulsions could be stabilised by sunflower DOS [18]. As expected, the rapeseed DOS were also surface-active at the air–water interface (Fig. 8A). The surface pressure induced by DOS was lower compared to that observed with WPI in the first 3 s, and showed a steeper increase afterwards. DOS led to a surface pressure around 31 mN/m after 3 h, which was almost twice higher than the final surface pressure reached with WPI. Mixing of WPI and DOS resulted in higher surface pressures than with pure WPI or DOS in the first 500 s of adsorption. Afterwards, the surface pressure followed the curve of pure DOS. It seems that WPI and DOS adsorbed at the interface in the initial phase, but DOS dominated the behaviour after 500 s. The exact composition of the interface was further examined by rheological experiments.

The DOS-stabilised interface had an E_d' between 19 and 20 mN/m over the whole range of amplitudes from 2 to 50%, with n = 0.30 for the power-law dependence of modulus on frequency (Table 1), and indicated a weaker and more mobile interface compared to WPI. The E_d' of WPI-DOS mixtures coincided with that measured for pure DOS, and also had a relative high *n*-value of 0.27. Shear rheology revealed that DOS and WPI-DOS-stabilised interfaces were too weak to be measured accurately, suggesting the formation of a very weak interface with little in-plane interactions between the molecules at the interface, comparable to the RPL-stabilised interface. The dominating behaviour of DOS in adsorption and rheological properties of the WPI-DOS mixture could be related to the displacement of whey proteins by DOS. The combination of Lissajous plots and microstructure imaging could help us further assess the stabilisation mechanism of both components at the air–water interface.

2.3.2. Lissajous plots and interfacial microstructure imaging

The Lissajous plots of DOS-stabilised films showed large differences from those of RPL; an overview of all Lissajous plots can be found in Figure S2 in the SI. The plots of RPL- and DOS-stabilised interfaces at 5% deformation exhibited a narrow ellipsoidal loop (Fig. 9A). At a higher deformation of 50%, the Lissajous plot of the DOS-stabilised films was narrower compared to that obtained for RPL, suggesting a more elastic-dominant behaviour. The Lissajous plot also exhibited strain softening in extension and compression to a lesser extent than the plot of an RPL-stabilised interface. Therefore, we expect the DOS to form a more cohesive interface compared to RPL. AFM images of LB films based on DOS at 15 mN/m showed a rather flat surface with higher structures that could be proteins, as DOS had a protein content of almost 70% (Fig. 9B). The presence of membrane proteins became more obvious at a higher compression to a surface pressure of 25 mN/m, where the microstructure became more dense and heterogeneous, as also observed in our previous work for a more diluted WPI system [24]. At such high compression, phospholipids could be pushed out of the surface, which would explain the strain softening between deformations of −0.35 and −0.50 in the Lissajous plot at 50% deformation amplitude.

A WPI-DOS-stabilised interface showed a Lissajous plot at 50% deformation that is even more tilted towards the horizontal axis compared to pure DOS, which indicates an even weaker interface. On the other hand, the strain softening in compression was not observed for WPI-DOS. The AFM image of the LB film at 15 mN/m (Fig. 9B) showed similar segregated WPI domains as on the WPI-RPL films (Fig. 6B). The WPI domains could be surrounded by DOS material, such as membrane proteins and phospholipids that dominated the interfacial properties, and this would explain

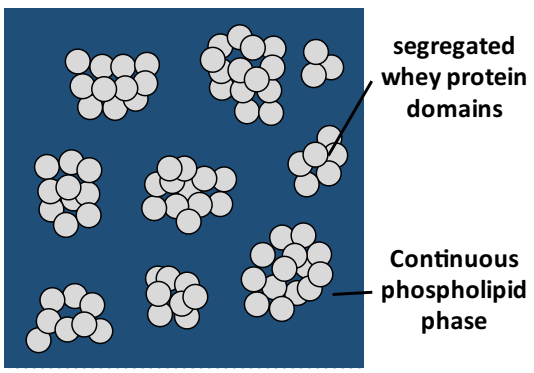

Fig. 7. Schematic representation (top view) of interfacial layer stabilised by WPI-RPL mixtures. Illustrations are not on-scale.

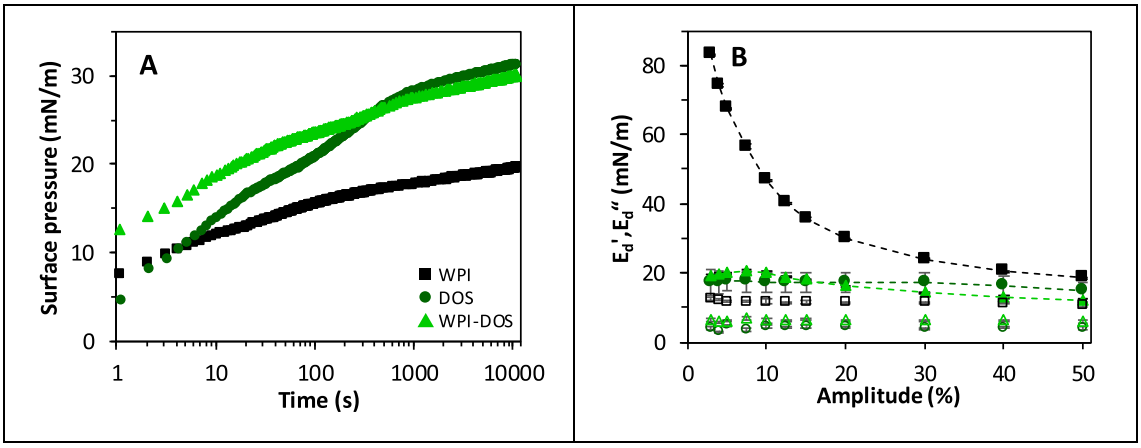

Fig. 8. (A) Surface pressure as a function of time of interfacial films stabilised by WPI (black square), DOS (dark green circle), and WPI-DOS mixtures (light green triangle) in buffer (20 mM PO_4, pH 7.0). The surface pressure isotherms represent an average from at least three replicates. The standard deviation was below 5%. (B) The surface dilatational storage (E_d') and loss (E_d") moduli as a function of amplitude of the interfaces mentioned in Fig. A. Closed symbols show the storage modulus (G_i' or E_d') and open symbols show the loss modulus (G_i" or E_d"). The averages and standard deviations are the result of at least three replicates. (For interpretation of the references to colour in this figure legend, the reader is referred to the web version of this article.)

the weak interfaces observed in dilatational and shear rheology. A schematic representation of a WPI-DOS mixed interface is shown in Fig. 10. At a higher surface pressure of 25 mN/m, the AFM image showed a similar microstructure with segregated whey protein domains. A slight change can be observed in the continuous phase between the domains, as more structures could be observed. The emerging structures could suggest the presence of membrane proteins in this phase, which started to segregate at higher compressions, as demonstrated in the AFM images of pure DOS films at a surface pressure of 25 mN/m. Increased segregation of membrane proteins might be reflected in the absence of the strain softening in compression in the Lissajous plot at 50% deformation amplitude, while the strain softening was present in the (50% deformation) plots of pure DOS-stabilised interfaces. Additionally, whey proteins might contribute to the overall interaction on the WPI-DOS-stabilised interface.

The WPI-DOS and WPI-RPL mixed interface showed the formation of segregated whey protein domains, surrounded by a continuous phase of either DOS (phospholipids and membrane proteins) or RPL (phospholipids). A major difference was the resistance against high compression/deformation, as RPL seemed to be pushed out of the interface, allowing whey proteins to interact, which did not occur for DOS. The higher protein content in DOS could have played a major role in this behaviour. The OS membrane proteins are known to be strongly anchored into the membrane, as membrane proteins form strong hydrophobic and electrostatic interactions with the phospholipids in the interfacial layer [21]. Membrane proteins could thus prevent the phospholipids in a DOS-stabilised interface from being expelled into the bulk upon (high) compression, while the expulsion of phospholipids did occur in an RPL-stabilised interface, where substantially fewer membrane proteins were present. A difference in in-plane molecular interactions is reflected in the surface pressure isotherms (Figure S1 in SI): for the DOS-based films, a change from an LE phase into an LC state without an LE-LC co-existence phase (slope increased after transition point at 29 mN/m), was observed, whereas the co-existence phase was present for the RPL-based film (slope decreased after transition point at 36 mN/m). The strong interactions between membrane proteins and phospholipids in the DOS is likely to contribute to the transition to a more condensed state upon compression. RPLs also adsorbed more slowly to the interface than whey proteins in the first 70 s. A slow adsorption behaviour would result in the presence of less RPL on the WPI-RPL interface, whereas more DOS might be present on the WPI-DOS interface. The membrane proteins seem to play a major role in the oleosome membrane by strongly interacting with phospholipids and, thereby, anchoring the phospholipids onto the interface. This would prevent the expulsion of phospholipids upon deformation of the interface.

2.4. Whey protein – oleosome mixtures

2.4.1. Adsorption behaviour and interfacial rheology of whey protein – oleosomes mixtures

Finally, we increased the complexity of the lipid components by using non-defatted oleosomes (OS), and the surface activity of OS, WPI and WPI-OS is shown in Fig. 11. The OS had an immediate increase of surface pressure, starting at 12 mN/m, and remained constant for about 10 s. Subsequently, the surface pressure increased rapidly for 200 s, followed by a more gradual increase to 25 mN/m after 3 h of adsorption time. Several studies already reported a high surface activity and the ability to stabilise interfaces for OS [14,18,19]. Waschatko et al. used Brewster angle microscopy to study the structure of an air–water interface stabilised by soybean OS in a Langmuir trough [19,20]. In this work, a slow initial adsorption phase of OS was observed, similar to our findings in Langmuir trough experiments (data not shown). The slow initial adsorption phase would explain the constant surface pressure in the first 10 s for OS in Fig. 11, and was followed by a rapid increase that could be related to the rupture of OS at the air–water interface. After the oleosome rupture, phospholipids, proteins and TAG are rearranging and forming phospholipid- and triacylglycerol (TAG)-rich regimes. The interfacial rearrangement phase could explain the slower increase of surface pressure after 200 s in Fig. 11. For sunflower OS, the rupture of OS was found to depend on the size, as OS larger than 1 μm ruptured at the oil–water interface, while oleosomes with a smaller diameter (<1 μm) remained intact [18]. The rupture of natural oil storage reservoir structures positioned at an air–water interface has also been demonstrated for low-density lipoproteins (LDL) from egg yolk, which consist of a lipid core surrounded by a phospholipid monolayer and membrane proteins [45,46]. The rupture of LDL and spreading of their phospholipids and membrane proteins was referred to as the main contributor to the emulsifying properties of egg yolk [47], thus suggesting a similarly prominent role of oleosome membrane components upon rupture. Mixing WPI and OS

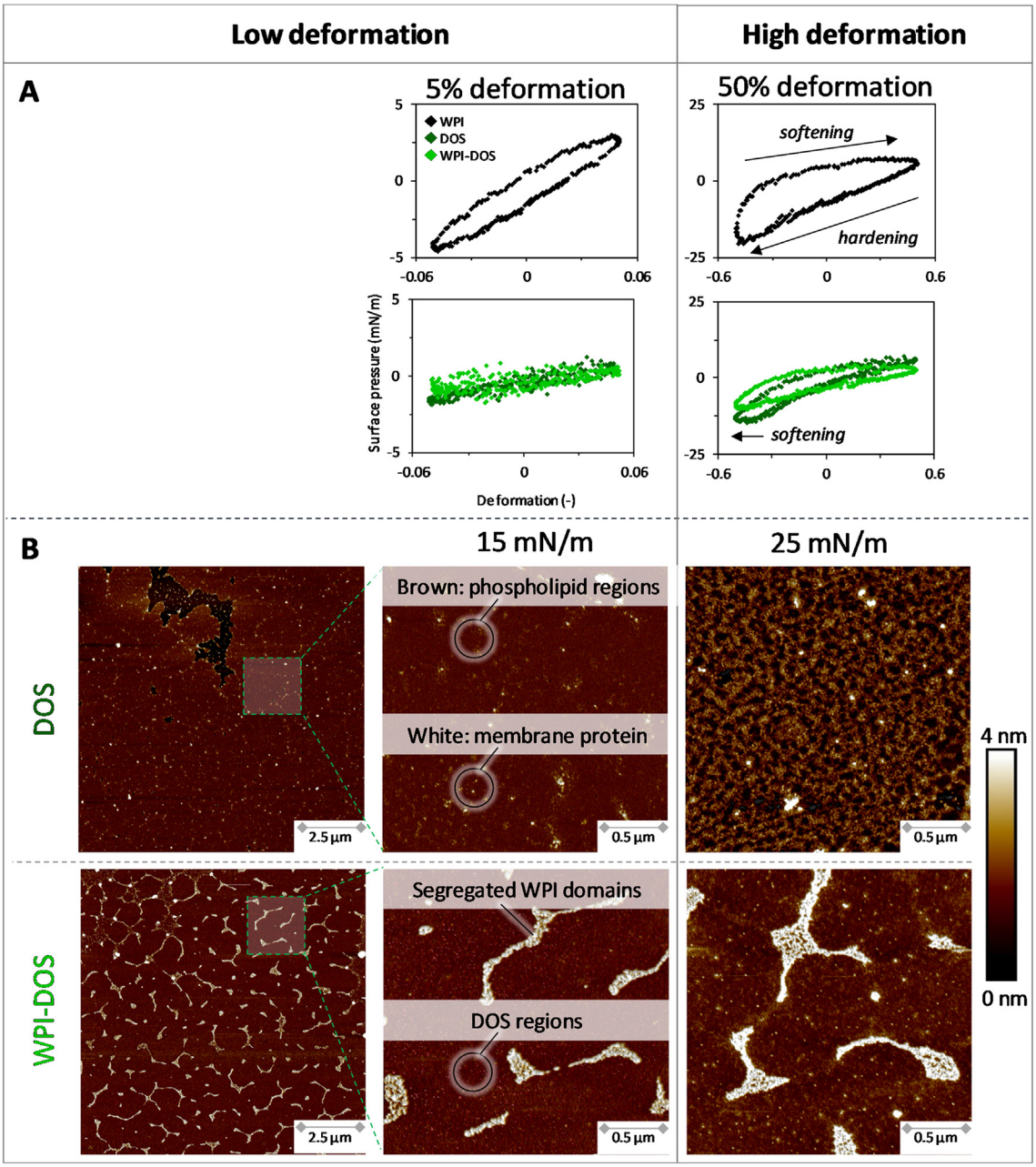

Fig. 9. (A) Lissajous plots of surface pressure as a function of the applied deformation, obtained from amplitude sweeps of air–water interfacial films stabilised by WPI, DOS, and WPI-DOS mixtures. For clarity, one representative plot is shown for each sample, but comparable plots were obtained on at least three replicates. (B) AFM images of Langmuir-Blodgett films made from DOS and WPI-DOS mixtures. The surface pressure indicates the conditions during film sampling.

resulted in a higher surface pressure increase in the first 3,000 s compared to pure WPI or OS, and had a final surface pressure of 24 mN/m. A higher surface pressure increase of the mixture suggests the co-adsorption of whey proteins and OS at the air–water interface. The interface stabilising mechanisms of WPI-OS mixtures were further assessed by performing surface rheology.

In surface shear rheology, the OS-stabilised interfaces were too weak to be measured accurately, which suggests the formation of a weak interface with limited in-plane interactions at the interface, as observed for RPL and DOS. We were able to obtain reliable values for the WPI-OS-stabilised interface (see Figure S3 in SI). The interface stabilised by the WPI-OS mixture had a modulus decrease of almost one order of magnitude, and a higher tanδ in the LVE regime (0.50–0.60) compared to pure whey protein-stabilised interfaces (tanδ = 0.24). The presence of OS caused whey proteins to form weaker and less solid-like interfaces, probably due to the disruption of the whey protein lateral network by the OS adsorbed material.

A comparable effect is present in the amplitude sweep in dilatational deformations (Fig. 11B). The moduli of OS-stabilised interfaces remained nearly constant over the entire range of amplitudes, and implied the formation of a weak and more stretchable interfacial layer. The whey protein-OS mixture-stabilised interface showed moduli close to those obtained with the pure OS, with an LVE regime up to 20% amplitude, followed by softening at higher deformations. The interactions at the interface were further studied by performing frequency sweeps, which resulted in *n*-values of 0.30 ± 0.01 and 0.18 ± 0.03 for OS and WPI-OS, respectively (Table 1). The moduli of OS-stabilised interfaces showed an increased frequency dependency, which revealed a more mobile

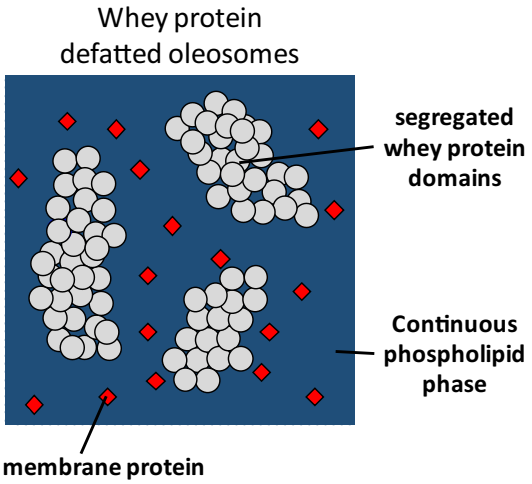

Fig. 10. Schematic representation (top view) of interfacial layer stabilised by WPI-DOS mixtures. Illustrations are not on-scale.

interface compared to films obtained with WPI and the WPI-OS mixture. A more mobile interface suggests increased mass transfer between interface and bulk, as observed for DOS and RPL interfaces. The exact interfacial composition was further analysed using Lissajous plots and microstructure imaging.

2.4.2. Lissajous plots and interfacial microstructure imaging

The 5% deformation Lissajous plots of the OS-stabilised interface had a symmetric and narrow loop, again suggesting a dominating elastic response (Fig. 12A). At 50% deformation, the shape of the plot was still narrow, but it exhibited a slight strain softening in compression. The strain softening occurred in the last part of the compression cycle between −0.30 and −0.50 deformation, which is likely to occur due to the exchange of stabiliser between bulk and interface, as the interface has a high frequency dependence and weak in-plane interactions. The AFM image of the OS-stabilised film at 15 mN/m was found to be highly complex (Fig. 12B, left). A magnified image of the surface allows us to evaluate the films in more detail (Fig. 12B, middle). In the images, a large flat and higher area is present (labelled as 'a'), which could be TAG-rich regions that were formed after rupturing of the OS at the interface. Rupture of the OS should yield fragments of the phospholipid/oleosin membrane, which could be the structures labelled as 'b'. Additionally, many smaller spherical structures between 50 and 200 nm are present in the film. At this point, we can only speculate about the nature of these structures that could be small OS or phospholipid-protein clusters. The AFM images are in agreement with the observations that larger oleosomes would rupture at an interface [18]. At a higher surface pressure of 25 mN/m, we observe a much flatter surface with fewer structures. Several spherical structures around 1 μm were present, which could be the TAG or phospholipid-rich regime. Overall, most of the structures observed at a surface pressure of 15 mN/m disappeared from the surface. From these images, it seems plausible that material is pushed out of the interface, either into the bulk or into a sub-layer (AFM only studies the topography of the interfacial microstructure, and cannot distinguish between these two). The rheological response of OS-stabilised interfaces confirms this scenario since the interfaces were found to be weak, stretchable and the response was significantly frequency-dependent. Based on the rheological properties and microstructure imaging, we drew a schematic representation of the adsorption process and structural rearrangements of OS at the air–water interface in Fig. 13.

The WPI-OS mixtures led to Lissajous plots similar to OS at a 5% deformation (Fig. 12A). Interestingly, the plots started to overlap more with those obtained with WPI at larger deformation, and at 50% deformation, the Lissajous plot obtained with WPI-OS coincided with the plot for WPI. Based on the adsorption isotherms, both whey proteins and OS are present at the interface (Fig. 11), and can also be observed in the AFM image at 15 mN/m that showed a different structure than for the films made with pure WPI or OS (Fig. 12B left). These images showed flat regions (labelled as 'c') surrounded by structures that largely resemble the protein clusters in WPI-based films (see magnified image). The flat regions could be phospholipid- or TAG-rich regimes, formed after rupturing of the oleosomes. Larger structures between 0.2 and 1 μm were also present and were presumed to be intact oleosomes. Submicron sunflower seed oleosomes were also found to be stable upon homogenisation and were even found to adsorb at the oil–water interface. Oleosomes between 1 and 5 μm were found to disrupt and participate in the interfacial layer, which is probably also occurring in our work. The exact stabilisation mechanism of the oleosomes related to droplet size has not been studied, but we assume that the membrane density plays a role in the oleosome stability against rupture. Larger oleosomes could possess a less dense membrane compared to smaller ones. A less dense mem-

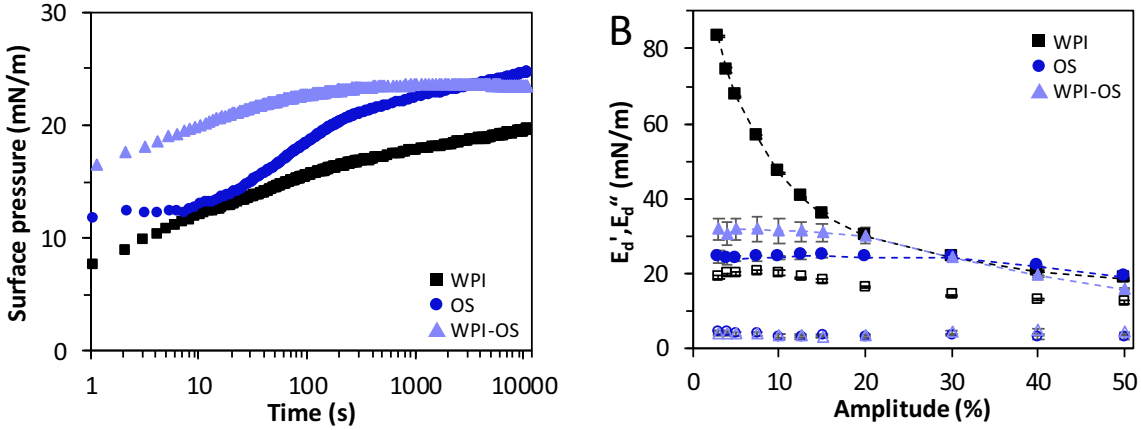

Fig. 11. (A) Surface pressure as a function of time of interfacial films stabilised by WPI (black square), OS (dark blue circle), and WPI-OS mixtures (light blue triangle) in buffer (20 mM PO_4, pH 7.0). The surface pressure isotherms represent an average from at least three replicates. The standard deviation was below 5%. (B) The surface dilatational storage (E_d') and loss (E_d") moduli as a function of amplitude of interfacial films stabilised by WPI (black square), OS (dark blue circle), and WPI-OS mixtures (light blue triangle) in buffer (20 mM PO_4, pH 7.0). Closed symbols show the storage modulus (E_d') and open symbols show the loss modulus (E_d"). The averages and standard deviations are the result of at least three replicates. (For interpretation of the references to colour in this figure legend, the reader is referred to the web version of this article.)

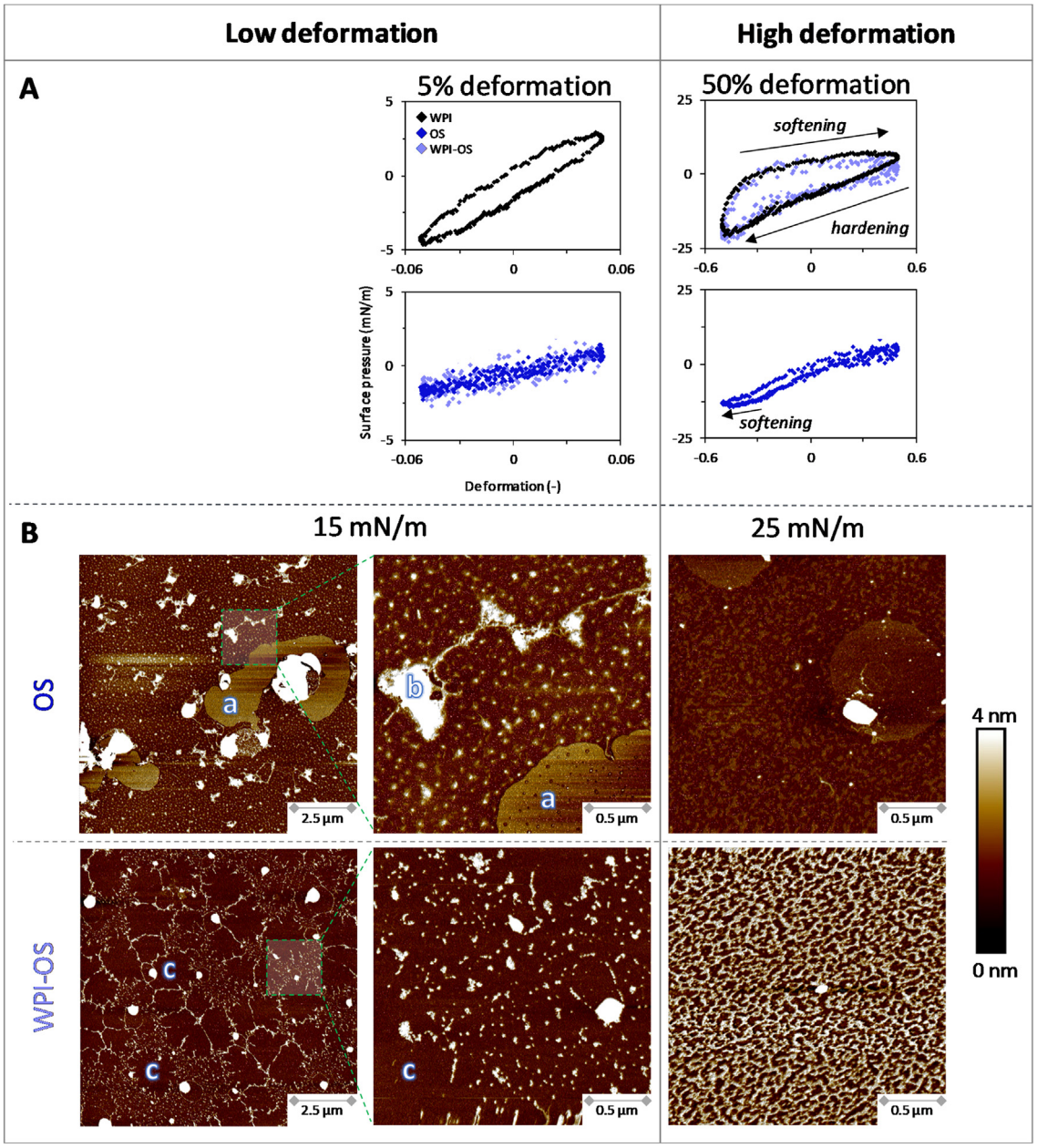

Fig. 12. (A) Lissajous plots of surface pressure as a function of the applied deformation, obtained during amplitude sweeps of air–water interfacial films stabilised by WPI, OS, and WPI-OS mixtures. For clarity, one representative plot is shown for each sample, but comparable plots were obtained on at least three replicates. (B) AFM images of Langmuir-Blodgett films made form WPI, OS, and WPI-OS mixtures. The surface pressure indicates the conditions during film sampling. TAG-rich regions are labelled as 'a'. Fragments of OS-membrane are labelled with 'b'. Phospholipid/TAG-rich regimes are labelled with 'c'.

brane could result in thinner areas, where oil could leak out. Upon leakage, the oleosome might start rupturing. These thinner areas on the membrane can also be formed upon deformation of the droplet, which is more likely to occur for larger oil droplets.

At a high surface pressure of 25 mN/m, an overall dense structure can be observed. This confirms that the clusters observed at low deformation were whey proteins, which started to jam and interact at a larger compression. At the same time, the OS material (TAG or phospholipids) might be pushed out of the interface or into a lower sublayer. Such a behaviour is confirmed by the Lissajous plots, where at low deformations, the OS seemed to dominate the response, and the rheological response of the WPI-OS mixture became WPI-dominated at higher deformations. To summarise, the WPI-OS mixture formed a mixed interface with domains of phospholipid/TAG-rich regimes, surrounded by whey protein clusters, as shown in the schematic representation in Fig. 14. As a result, co-adsorption of both OS and WPI would largely impair the interactions among adsorbed proteins at the air–water interface, which is also shown for mixtures of WPI and RPL or DOS.

The interface stabilising behaviour of WPI-OS and WPI-RPL mixed films showed similarities, as the lipids were pushed out upon compression, and whey proteins started to interact, as shown in the rheology, especially at large deformations of 50% deformation amplitude. It seemed that more lipids were pushed out of the WPI-OS films compared to WPI-RPL, as substantially more whey protein clusters were present on the WPI-OS film at higher compression. We attribute such a behaviour to the presence of TAG-rich regions at the WPI-OS mixtures, which could be easily pushed into the bulk or below the surface upon compression, as little lateral interaction is expected between the TAGs. If TAGs are

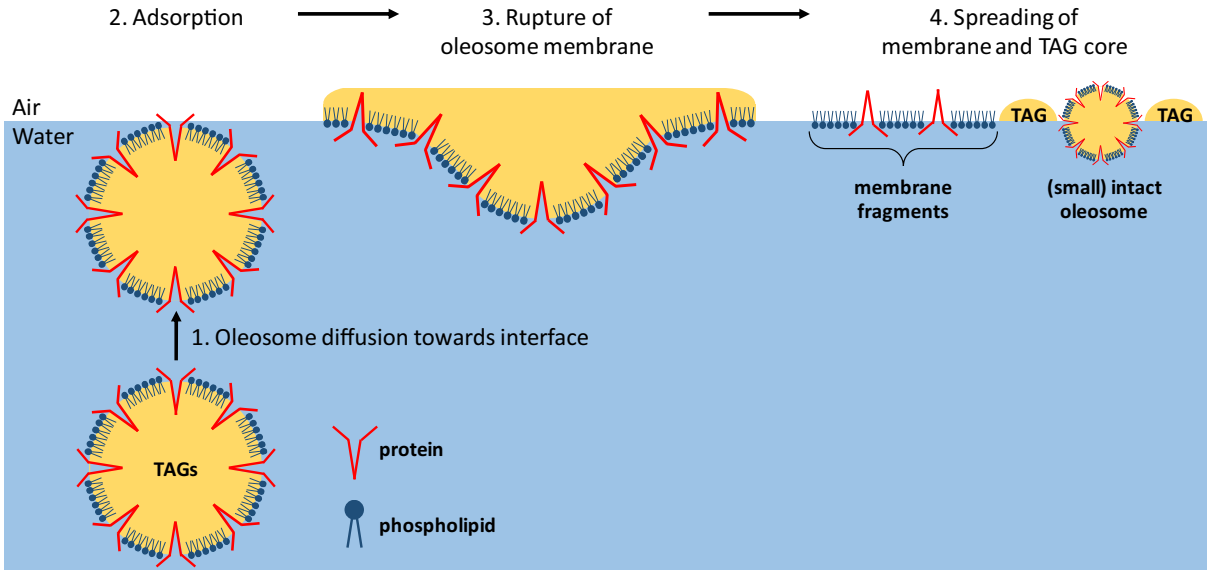

Fig. 13. Schematic representation of adsorption of OS and structural rearrangements at the air–water interface. Illustrations are not on-scale.

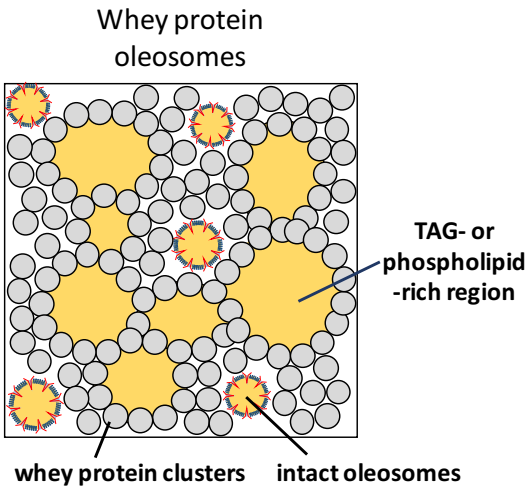

Fig. 14. Schematic representation (top view) of interfacial layer stabilised by WPI-OS mixtures. Illustrations are not on-scale.

pushed into the bulk, we would expect a transition in a colloidal state, as free lipids in a polar phase would be thermodynamically unfavourable. Droplets of TAGs could be stabilised by excess interfacial stabilisers (protein or phospholipids) in the bulk. We should also keep in mind that the membrane material (phospholipids and proteins) was lower in OS compared to DOS or RPL due to the presence of TAGs, as all lipid extracts were standardised on dry matter.

2.5. Step-dilatation

The interfacial films stabilised by WPI and rapeseed lipids were further analysed by performing step-dilatations in the drop tensiometer by suddenly expanding the interfacial area by 10%. The sudden expanding step resulted in a relaxation response, which depends on the stiffness and mobility of the formed interfacial layer. The relaxation response was fitted using equation (1), which is a combination of a Kohlraus-William-Watts stretch exponential and a regular exponential term. The KWW model described the relaxation behaviour of the interface, while the second term was included to decouple the ageing of the interface from the relaxation process.

$$\gamma(t) = ae^{-(t/\tau_1)^{\beta}} + be^{-t/\tau_2} + c \quad (1)$$

The stretch exponent β and relaxation time τ_1 are reported in Table 2. Other values are the characteristic time of the second term τ_1 and fitting parameters a, b, and c, and can be found in Table S1 in the SI.

The stretch exponent β was between 0.51 and 0.64 for all interfaces. A β-value below 1 suggests dynamic heterogeneity in the relaxation response, which could be the result of local variations in the relaxation kinetics, thus leading to a wide distribution of relaxation times. β-values between 0.52 and 0.68 have been observed for a wide range of protein-stabilised interfaces [24,37,48]. The occurrence of dynamic heterogeneity was closely related to structural heterogeneity of the interfacial microstructure, as also observed for the interfaces studied in this work.

A significant difference was observed in the relaxation times τ_1: RPL-, DOS- and OS-stabilised films showed relaxation times around 11 s, whereas films made of WPI-lipid mixtures showed relaxation times between 11.2 and 18.5 s. The whey protein-stabilised interface had the highest relaxation time of 25.9 s, which was expected as whey proteins formed stiff and solid-like interfacial layers, also with a low frequency-dependence (n = 0.12) in dilatational deformations (Table 1). The pure lipid (RPL, DOS and OS) and WPI-lipid-stabilised interface had lower relaxation times, showing a more mobile interfacial layer, and was also confirmed by the *n*-values (0.18–0.30). The more mobile interfaces were also in line with

Table 2
The β and τ_1 values for interfaces prepared with WPI, OS, DOS, RPL, and mixtures of WPI-OS, WPI-DOS, WPI-RPL at 10% extension. Other variables can be found in Table S1 in the SI. The averages and standard deviations are the result of at least three replicates.

	β	τ_1 (s)
WPI	0.51 ± 0.05	25.9 ± 2.6
OS	0.56 ± 0.04	11.3 ± 1.5
WPI-OS	0.61 ± 0.04	14.7 ± 4.9
DOS	0.54 ± 0.10	11.3 ± 2.8
WPI-DOS	0.64 ± 0.01	18.5 ± 1.9
RPL	0.58 ± 0.04	10.7 ± 2.1
WPI-RPL	0.60 ± 0.01	11.2 ± 3.6

the rheological responses, as the lipid-stabilised interfaces exhibited predominantly elastic responses with weak in-plane interactions. At a step-dilatation of 10% area deformation, the lipids also affected the interfaces stabilised by the WPI-lipid mixtures, as the relaxation times were lower than pure WPI. The WPI-RPL interface had a similar relaxation time around 11 s, suggesting the earlier mentioned dominating rheological behaviour of RPL in WPI-RPL mixtures at low deformation. WPI-OS-stabilised interfaces had a slightly higher relaxation time (15 s) compared to the pure OS-stabilised interface. The slight increase of relaxation time could be due to the whey protein domains on the WPI-OS-stabilised interface that contributed to a slightly increased resistance in the relaxation response. The whey protein clusters in WPI-OS (Fig. 12) were also more widely distributed over the interface compared to those in the WPI-RPL system (Fig. 6), which were segregated into domains. This would cause the whey protein clusters in the WPI-OS-stabilised films to interact at a lower compression than for the WPI-RPL films, which was also shown in the AFM images, as the WPI-OS films at a high compression (25 mN/m, Fig. 12) showed a much denser structure with more whey protein clusters compared to the WPI-RPL system (Fig. 6). Finally, the WPI-DOS-stabilised interfaces had a higher relaxation time of 19 s. At a higher compression at 25 mN/m, the AFM image of WPI-DOS films (Fig. 9) showed more segregated structures compared to pure DOS-based films, which was also reflected in the disappearance of strain softening in compression in the 50% deformation Lissajous plot of the WPI-DOS-based film. This might imply that whey proteins contribute to the overall interaction on the WPI-DOS-stabilised interface, thereby increasing the relaxation time. In general, we demonstrated that rapeseed lipids largely dominate the interfacial properties of WPI-lipid mixtures.

3. Conclusion

In this work, we characterised interfacial films stabilised by whey proteins (WPI), rapeseed lipids, and WPI-lipid mixtures. Whey proteins formed stiff interfacial layers that behaved as viscoelastic solids, while rapeseed oleosomes (OS) formed weak and stretchable interfacial layers. The adsorption and proposed interface stabilisation mechanisms are shown in Fig. 13. The OS membrane was found to rupture at the air–water interface, followed by the spreading of the membrane components (phospholipids and proteins) and the triacylglycerol (TAG) core. As a result, TAG- and phospholipid-rich regions were formed, as shown in AFM images of Langmuir-Blodgett films. Additionally, the smaller intact OS seemed to be present in the films. Whey proteins and lipids were also used concomitantly. The AFM images of films made of WPI-OS mixtures showed a mixed interface of WPI and OS, where regions of phospholipid or TAG from OS were surrounded by clusters of whey proteins. As a result, the OS dominated the rheological response at low deformations. At higher deformations, the lipids were pushed out, and the WPI started to dictate the mechanical properties of the interface.

The influence of OS membrane components was also studied by incorporating a defatted oleosome (DOS) extract and a rapeseed phospholipid extract (RPL). Mixtures of WPI and DOS showed a continuous phase of phospholipids or membrane fragments, and domains of segregated whey proteins could be observed. The continuous phase dominated the rheological response over the entire range of tested deformations. The last included sample was rapeseed phospholipids (RPL). At low deformations, the RPL dominated the rheological response in WPI-RPL mixtures, as the microstructure of the interface was found to coincide with that of the WPI-DOS system. A distinct difference was observed at higher deformations for WPI-RPL mixtures, where whey proteins started to dominate the rheological response, as the protein-rich regions started jamming and interacting, just like with the WPI-OS mixture. It appeared that the presence of OS membrane proteins influences the rheological properties induced by the lipids, probably by interactions with the phospholipids, thus increasing the resistance against deformation. From this, we conclude that whey proteins and rapeseed lipids form mixed interfaces. Processing of the lipids can largely influence the composition (protein/phenol/TAG) and the state of the lipids, and these properties determine the interface stabilising properties of the lipid extracts.

Our work provided new insights on the interface stabilising properties of OS and their membrane constituents, and especially in mixture with proteins. The OS seem to possess similar interface stabilising properties as RPL, a widely used emulsifier, and the properties of both lipid sources in a mixture with proteins were found to be remarkably similar. Therefore, OS could play a role as a more sustainable alternative for phospholipids (lecithin) as emulsifiers. Another important finding is that the oleosomes hinder the network formation of whey proteins, which could lead to weaker interfacial layers. Such behaviour could impair interface stabilising properties of proteins in macroscopic systems, such as foams and emulsions. The weakening effect of oleosomes should receive more attention in macroscopic systems, and also be taken into account when designing food systems with oleosomes. Our findings are an important step to further explore the potential of oleosomes as sustainable ingredients and interface stabilisers in food systems.

CRediT authorship contribution statement

Jack Yang: Conceptualization, Investigation, Methodology, Validation, Visualization, Writing - original draft. **Leonie C. Waardenburg:** Investigation, Methodology. **Claire C. Berton-Carabin:** Writing - review & editing, Methodology, Conceptualization. **Constantinos V. Nikiforidis:** Conceptualization, Methodology, Writing - review & editing. **Erik van der Linden:** Writing - review & editing, Funding acquisition. **Leonard M.C. Sagis:** Conceptualization, Methodology, Supervision, Writing - review & editing.

Declaration of Competing Interest

The authors declare that they have no known competing financial interests or personal relationships that could have appeared to influence the work reported in this paper.

Acknowledgements

The authors have declared that no competing interest exists. The project is funded by TiFN, a public-private partnership on precompetitive research in food and nutrition. The public partners are responsible for the study design, data collection and analysis, decision to publish, and preparation of the manuscript. The private partners have contributed to the project through regular discussion. This research was performed with additional funding from the Netherlands Organisation for Scientific Research (NWO), and the Top Consortia for Knowledge and Innovation of the Dutch Ministry of Economic Affairs (TKI). NWO project number: ALWTF.2016.001.

Appendix A. Supplementary material

Supplementary data to this article can be found online at https://doi.org/10.1016/j.jcis.2021.05.172.

References

[1] J.T.C. Tzen, Integral Proteins in Plant Oil Bodies, ISRN Bot. 2012 (2012) 1–16, https://doi.org/10.5402/2012/173954.

[2] C.V. Nikiforidis, Structure and Functions of Oleosomes (Oil Bodies), Adv. Colloid Interf. Sci. 274 (2019), https://doi.org/10.1016/j.cis.2019.102039 102039.

[3] G.I. Frandsen, J. Mundy, J.T.C. Tzen, Oil Bodies and Their Associated Proteins Oleosin and Caleosin, Physiol. Plant. 112 (3) (2001) 301–307, https://doi.org/10.1034/j.1399-3054.2001.1120301.x.

[4] J.T.C. Tzen, A.H.C. Huang, Surface Structure and Properties of Plant Seed Oil Bodies, J. Cell Biol. 117 (2) (1992) 327–335, https://doi.org/10.1083/jcb.117.2.327.

[5] J.T.C. Tzen, Y.Z. Cao, P. Laurent, C. Ratnayake, A.H.C. Huang, Lipids, Proteins, and Structure of Seed Oil Bodies from Diverse Species, Plant Physiol. 101 (1) (1993) 267–276, https://doi.org/10.1104/pp.101.1.267.

[6] R. Pichot, R.L. Watson, I.T. Norton, Phospholipids at the Interface: Current Trends and Challenges, Int. J. Mol. Sci. 14 (6) (2013) 11767–11794, https://doi.org/10.3390/ijms140611767.

[7] P.J.M. Pelgrom, R.M. Boom, M.A.I. Schutyser, Functional Analysis of Mildly Refined Fractions from Yellow Pea, Food Hydrocoll. 44 (2014) 12–22, https://doi.org/10.1016/j.foodhyd.2014.09.001.

[8] J. Yang, I. Faber, C.C. Berton-Carabin, C.V. Nikiforidis, E. van der Linden, L.M.C. Sagis, Foams and Air-Water Interfaces Stabilised by Mildly Purified Rapeseed Proteins after Defatting, Food Hydrocoll. 112 (2020), https://doi.org/10.1016/j.foodhyd.2020.106270 106270.

[9] M.E.J. Geerts, E. Mienis, C.V. Nikiforidis, A. van der Padt, A.J. van der Goot, Mildly Refined Fractions of Yellow Peas Show Rich Behaviour in Thickened Oil-in-Water Emulsions, Innov. Food Sci. Emerg. Technol. 41 (2017) 251–258, https://doi.org/10.1016/j.ifset.2017.03.009.

[10] O.A. Karkani, N. Nenadis, C.V. Nikiforidis, V. Kiosseoglou, Effect of Recovery Methods on the Oxidative and Physical Stability of Oil Body Emulsions, Food Chem. 139 (1–4) (2013) 640–648, https://doi.org/10.1016/j.foodchem.2012.12.055.

[11] V.N. Kapchie, L. Yao, C.C. Hauck, T. Wang, P.A. Murphy, Oxidative Stability of Soybean Oil in Oleosomes as Affected by PH and Iron, Food Chem. 141 (3) (2013) 2286–2293, https://doi.org/10.1016/j.foodchem.2013.05.018.

[12] J. Ding, Z. Xu, B. Qi, Z. Liu, L. Yu, Z. Yan, L. Jiang, X. Sui, Thermally Treated Soya Bean Oleosomes: The Changes in Their Stability and Associated Proteins, Int. J. Food Sci. Technol. 55 (1) (2020) 229–238, https://doi.org/10.1111/ijfs.14266.

[13] J. Ding, J. Wen, J. Wang, R. Tian, L. Yu, L. Jiang, Y. Zhang, X. Sui, The Physicochemical Properties and Gastrointestinal Fate of Oleosomes from Non-Heated and Heated Soymilk, Food Hydrocoll. 2020 (100) (October 2019), https://doi.org/10.1016/j.foodhyd.2019.105418 105418.

[14] T. Ishii, K. Matsumiya, Y. Nambu, M. Samoto, M. Yanagisawa, Y. Matsumura, Interfacial and Emulsifying Properties of Crude and Purified Soybean Oil Bodies, Food Struct. 12 (2017) 64–72, https://doi.org/10.1016/j.foostr.2016.12.005.

[15] M.J. Romero-Guzmán, N. Köllmann, L. Zhang, R.M. Boom, C.V. Nikiforidis, Controlled Oleosome Extraction to Produce a Plant-Based Mayonnaise-like Emulsion Using Solely Rapeseed Seeds, Lwt (123) (2020), https://doi.org/10.1016/j.lwt.2020.109120. August 2019 109120.

[16] B.I. Zielbauer, A.J. Jackson, S. Maurer, G. Waschatko, M. Ghebremedhin, S.E. Rogers, R.K. Heenan, L. Porcar, T.A. Vilgis, Soybean Oleosomes Studied by Small Angle Neutron Scattering (SANS), J. Colloid Interf. Sci. 529 (2018) 197–204, https://doi.org/10.1016/j.jcis.2018.05.080.

[17] D. Iwanaga, D.A. Gray, I.D. Fisk, E.A. Decker, J. Weiss, D.J. McClements, Extraction and Characterization of Oil Bodies from Soy Beans: A Natural Source of Pre-Emulsified Soybean Oil, J. Agric. Food Chem. 55 (21) (2007) 8711–8716, https://doi.org/10.1021/jf071008w.

[18] D. Karefyllakis, A.J. Van Der Goot, C.V. Nikiforidis, The Behaviour of Sunflower Oleosomes at the Interfaces, Soft Matter 15 (23) (2019) 4639–4646, https://doi.org/10.1039/c9sm00352e.

[19] G. Waschatko, A. Junghans, T.A. Vilgis, Soy Milk Oleosome Behaviour at the Air-Water Interface, Faraday Discuss. 158 (2012) 157–169, https://doi.org/10.1039/c2fd20036h.

[20] Waschatko, G.; Schiedt, B.; Vilgis, T. A.; Junghans, A. Soybean Oleosomes Behavior at the Air − Water Interface. J. Phys. Chem. B 2012, 116 (10832–10841). https://doi.org/10.1021/jp211871v.

[21] M. Deleu, G. Vaca-Medina, J.F. Fabre, J. Roïz, R. Valentin, Z. Mouloungui, Interfacial Properties of Oleosins and Phospholipids from Rapeseed for the Stability of Oil Bodies in Aqueous Medium, Colloids Surf. B Biointerf. 80 (2) (2010) 125–132, https://doi.org/10.1016/j.colsurfb.2010.05.036.

[22] J.P.D. Wanasundara, T.C. McIntosh, S.P. Perera, T.S. Withana-Gamage, P. Mitra, Canola/Rapeseed Protein-Functionality and Nutrition, *Ocl* 23 (4) (2016) D407, https://doi.org/10.1051/ocl/2016028.

[23] E. Dickinson, Adsorbed Protein Layers at Fluid Interfaces: Interactions, Structure and Surface Rheology, Colloids Surf. B Biointerf. 15 (2) (1999) 161–176, https://doi.org/10.1016/S0927-7765(99)00042-9.

[24] J. Yang, I. Thielen, C.C. Berton-Carabin, E. van der Linden, L.M.C. Sagis, Nonlinear Interfacial Rheology and Atomic Force Microscopy of Air-Water Interfaces Stabilized by Whey Protein Beads and Their Constituents, Food Hydrocoll. 101 (2020), https://doi.org/10.1016/j.foodhyd.2019.105466 105466.

[25] J. Yang, S.P. Lamochi Roozalipour, C.C. Berton-Carabin, C.V. Nikiforidis, E. van der Linden, L.M.C. Sagis, Air-Water Interfacial and Foaming Properties of Whey Protein - Sinapic Acid Mixtures, Food Hydrocoll. 112 (2021), https://doi.org/10.1016/j.foodhyd.2020.106467 106467.

[26] Romero-guzman, M. J.; Louis, L. J.; Kyriakopoulou, K.; Boom, R. M.Nikiforidis, C. V. Efficient Single-Step Rapeseed Oleosome Extraction Using Twin-Screw Press. 2020, 276. https://doi.org/10.1016/j.jfoodeng.2019.109890.

[27] A. Fetzer, T. Herfellner, P. Eisner, Rapeseed Protein Concentrates for Non-Food Applications Prepared from Pre-Pressed and Cold-Pressed Press Cake via Acidic Precipitation and Ultrafiltration, Ind. Crops Prod. 132 (2019) 396–406, https://doi.org/10.1016/j.indcrop.2019.02.039.

[28] S. Vandebril, A. Franck, G.G. Fuller, P. Moldenaers, J. Vermant, A Double Wall-Ring Geometry for Interfacial Shear Rheometry, Rheol. Acta 49 (2) (2010) 131–144, https://doi.org/10.1007/s00397-009-0407-3.

[29] J.P.D. Wanasundara, S.J. Abeysekara, T.C. McIntosh, K.C. Falk, Solubility Differences of Major Storage Proteins of Brassicaceae Oilseeds, JAOCS J. Am. Oil Chem. Soc. 89 (5) (2012) 869–881, https://doi.org/10.1007/s11746-011-1975-9.

[30] J. Maldonado-Valderrama, J.M.R. Patino, Interfacial Rheology of Protein-Surfactant Mixtures, Curr. Opin. Colloid Interf. Sci. 15 (4) (2010) 271–282, https://doi.org/10.1016/j.cocis.2009.12.004.

[31] D.J. McClements, C.E. Gumus, Natural Emulsifiers — Biosurfactants, Phospholipids, Biopolymers, and Colloidal Particles: Molecular and Physicochemical Basis of Functional Performance, Adv. Colloid Interf. Sci. 234 (2016) 3–26, https://doi.org/10.1016/j.cis.2016.03.002.

[32] E. Hildebrandt, H. Nirschl, R.J. Kok, G. Leneweit, Adsorption of Phospholipids at Oil/Water Interfaces during Emulsification Is Controlled by Stress Relaxation and Diffusion, Soft Matter 14 (19) (2018) 3730–3737, https://doi.org/10.1039/c8sm00005k.

[33] K. Hyun, S.H. Kim, K.H. Ahn, S.J. Lee, Large Amplitude Oscillatory Shear as a Way to Classify the Complex Fluids, J. Nonnewton. Fluid Mech. 107 (2002) 51–65, https://doi.org/10.1016/S0377-0257(02)00141-6.

[34] J. Lucassen, M. Van Den Tempel, Dynamic Measurements of Dilational Properties of a Liquid Interface, Chem. Eng. Sci. 27 (6) (1972) 1283–1291, https://doi.org/10.1016/0009-2509(72)80104-0.

[35] L.M.C. Sagis, K.N.P. Humblet-Hua, S.E.H.J. van Kempen, Nonlinear Stress Deformation Behavior of Interfaces Stabilized by Food-Based Ingredients, J. Phys.-Condensed Matter 26 (46) (2014) 9, https://doi.org/10.1088/0953-8984/26/46/464105.

[36] Ewoldt, R. H.; Hosoi, A. E.; McKinley, G. H. New Measures for Characterizing Nonlinear Viscoelasticity in Large Amplitude Oscillatory Shear. J. Rheol. (N. Y. N. Y). 2007, 52 (6), 1427–1458. https://doi.org/10.1122/1.2970095.

[37] L.M.C. Sagis, B. Liu, Y. Li, J. Essers, J. Yang, A. Moghimikheirabadi, E. Hinderink, C. Berton-Carabin, K. Schroen, Dynamic Heterogeneity in Complex Interfaces of Soft Interface-Dominated Materials, Sci. Rep. 9 (1) (2019) 1–12, https://doi.org/10.1038/s41598-019-39761-7.

[38] V.M. Kaganer, H. Hohwald, P. Dutta, Structure and Phase Transitions in Langmuir Monolayers Pdf, Rev. Mod. Phys. 71 (3) (1999) 779–819, https://doi.org/10.1103/RevModPhys.71.779.

[39] P.A. Rühs, N. Scheuble, E.J. Windhab, P. Fischer, Protein Adsorption and Interfacial Rheology Interfering in Dilatational Experiment, Eur. Phys. J. Spec. Top. 222 (1) (2013) 47–60, https://doi.org/10.1140/epjst/e2013-01825-0.

[40] C.J. Beverung, C.J. Radke, H.W. Blanch, Protein Adsorption at the Oil/Water Interface: Characterization of Adsorption Kinetics by Dynamic Interfacial Tension Measurements, Biophys. Chem. 81 (1) (1999) 59–80, https://doi.org/10.1016/S0301-4622(99)00082-4.

[41] G. Giménez-Ribes, M. Habibi, L.M.C. Sagis, Interfacial Rheology and Relaxation Behavior of Adsorption Layers of the Triterpenoid Saponin Escin, J. Colloid Interf. Sci. 563 (2020) 281–290, https://doi.org/10.1016/j.jcis.2019.12.053.

[42] K. Golemanov, S. Tcholakova, N. Denkov, E. Pelan, S.D. Stoyanov, Remarkably High Surface Visco-Elasticity of Adsorption Layers of Triterpenoid Saponins, Soft Matter. 9 (24) (2013) 5738, https://doi.org/10.1039/c3sm27950b.

[43] A.R. Mackie, A.P. Gunning, P.J. Wilde, V.J. Morris, Orogenic Displacement of Protein from the Air/Water Interface by Competitive Adsorption, J. Colloid Interf. Sci. 210 (1) (1999) 157–166, https://doi.org/10.1006/jcis.1998.5941.

[44] A. Mackie, P. Wilde, The Role of Interactions in Defining the Structure of Mixed Protein-Surfactant Interfaces, Adv. Colloid Interf. Sci. 117 (1–3) (2005) 3–13, https://doi.org/10.1016/j.cis.2005.04.002.

[45] S. Dauphas, V. Beaumal, A. Riaublanc, M. Anton, Hen Egg Yolk Low-Density Lipoproteins Film Spreading at the Air - Water and Oil - Water Interfaces, J. Agric. Food Chem. 54 (10) (2006) 3733–3737, https://doi.org/10.1021/jf053174e.

[46] S. Dauphas, V. Beaumal, P. Gunning, A. Mackie, P. Wilde, V. Vié, A. Riaublanc, M. Anton, Structure Modification in Hen Egg Yolk Low Density Lipoproteins Layers between 30 and 45 MN/m Observed by AFM, Colloids Surf. B Biointerf. 54 (2) (2007) 241–248, https://doi.org/10.1016/j.colsurfb.2006.10.027.

[47] M. Anton, Egg Yolk: Structures, Functionalities and Processes, J. Sci. Food Agric. 93 (12) (2013) 2871–2880, https://doi.org/10.1002/jsfa.6247.

[48] P. Cicuta, Compression and Shear Surface Rheology in Spread Layers of β-Casein and β-Lactoglobulin, J. Colloid Interf. Sci. 308 (1) (2007) 93–99, https://doi.org/10.1016/j.jcis.2006.12.056.